Earth and Planetary Science Letters 513 (2019) 20–28

Contents lists available at ScienceDirect

Earth and Planetary Science Letters

www.elsevier.com/locate/epsl

Dominant influence of the humidity in the moisture source region on the ^{17}O-excess in precipitation on a subtropical island

Yuina Uechi, Ryu Uemura *

Department of Chemistry, Biology, and Marine Science, University of the Ryukyus, 1 Senbaru, Nishihara, Okinawa, 903-0213, Japan

ARTICLE INFO

Article history:
Received 23 August 2018
Received in revised form 20 December 2018
Accepted 10 February 2019
Available online 25 February 2019
Editor: J. Adkins

Keywords:
triple oxygen isotopes
^{17}O-excess
precipitation
subtropical hydrological cycle
d-excess
Asian monsoon

ABSTRACT

A high-precision analysis of the triple oxygen isotope composition of water provides a new tracer denoted as ^{17}O-excess. Early theoretical and experimental studies suggest that changes in the ^{17}O-excess in precipitation can be interpreted as variations in the relative humidity in moisture source regions for precipitation. However, subsequent studies on ^{17}O-excess in the precipitation in polar and dry regions suggest the importance of additional fractionation, such as snow formation and raindrop re-evaporation processes, which diminish the relative humidity information in oceanic source regions. To date, whether humidity in the moisture source region can be quantified based on observations of ^{17}O-excess in precipitation has not been proven. Here, we show a two-year record of the ^{17}O-excess in precipitation on a maritime island in the East Asian monsoon region. The normalized relative humidity in the source region was reconstructed from ^{17}O-excess data using a simple evaporation model. We demonstrate that the reconstructed relative humidity is quantitatively consistent with observations in the oceanic moisture source region. This result suggests that the ^{17}O-excess in precipitation on the subtropical island is determined largely by diffusional fractionation during evaporation in the ocean. We also test the impact of a possibly different ^{17}O–^{18}O slope suggested by a recent study on the ^{17}O-excess definition. This different definition results in a minor impact on the data from tropical and subtropical regions but a significant change in the data from polar regions. These results suggest that the ^{17}O-excess in precipitation in tropical and subtropical regions is a unique quantitative tracer for the relative humidity in oceanic moisture source regions and thus will be a useful tracer and proxy for hydrological and paleoclimate studies.

1. Introduction

The oxygen and hydrogen isotope ratios (δ^{18}O and δD, respectively) in precipitation have been widely used as tracers of the water cycle (e.g., Dansgaard, 1964). A combination of these two isotope ratios generates a moisture source parameter, namely, the deuterium excess (d-excess = δD–8 δ^{18}O) (Dansgaard, 1964), which originates from diffusional fractionation during evaporation and is expressed as a non-zero intercept of the global meteoric water line (Craig, 1961). An isotopic model predicts that d-excess can effectively reflect the relative humidity and sea surface temperature (SST) in oceanic moisture sources (Merlivat and Jouzel, 1979); this theory is generally supported by observations of water vapor in the boundary layer (Benetti et al., 2015; Steen-Larsen et al., 2014b; Uemura et al., 2008).

A new parameter known as ^{17}O-excess has been established based on recent developments in the acquisition of high-precision measurements of the ^{17}O/^{16}O ratio, namely, δ^{17}O (Angert et al., 2004; Barkan and Luz, 2005). Analogous to d-excess, an excess of δ^{17}O in a δ^{17}O–δ^{18}O plot results from diffusional isotopic fractionation during evaporation in the ocean; furthermore, theory and experimentation both suggest that ^{17}O-excess reflects variations in the relative humidity at the ocean surface in the moisture source region and that the temperature dependence of ^{17}O-excess is smaller than that of d-excess (Barkan and Luz, 2005; Barkan and Luz, 2007; Luz and Barkan, 2010). In fact, an observation of the atmospheric water vapor over the ocean showed that ^{17}O-excess exhibits a negative correlation with the relative humidity (Uemura et al., 2010).

Because the δ^{18}O and δD of water in polar ice cores contain invaluable information on past hydroclimatic changes (e.g., Jouzel, 2013; Uemura et al., 2018), many studies have attempted to reveal ^{17}O-excess variations in polar regions (e.g., Landais et al., 2008; Risi et al., 2010; Steen-Larsen et al., 2014a). In a pioneering investigation, the ^{17}O-excess variations over glacial cycles in the Antarctic

* Corresponding author.
E-mail address: ruemura@sci.u-ryukyu.ac.jp (R. Uemura).

https://doi.org/10.1016/j.epsl.2019.02.012
0012-821X/

Vostok ice core were interpreted as changes in the relative humidity normalized to the SST and/or wind speed in the moisture source region (Landais et al., 2008). Ice cores from coastal sites suggest that ^{17}O-excess values at inland sites such as Vostok may be highly sensitive to local effects (Winkler et al., 2012); in inland areas, the ^{17}O-excess of snow decreases due to isotopic fractionation during the formation of snow (Pang et al., 2015; Touzeau et al., 2016). In conjunction with isotope modeling, ice core data from West Antarctica suggest a limited role of changes in the relative humidity in determining the glacial–interglacial changes in the Antarctic ^{17}O-excess (Schoenemann et al., 2014). Most recently, Miller (2018) suggested that the precipitation regime has a substantial influence on Antarctic precipitation. In summary, the findings of previous studies suggest that ^{17}O-excess data in ice cores can be interpreted in multiple ways.

In addition to those in polar regions, hydroclimatic changes in tropical and subtropical regions are also crucial for understanding the mechanism of natural climate change. Analogous to those of ice cores, the isotopic compositions of past rainwater in tropical and subtropical regions are preserved within fluid inclusions trapped in speleothems (e.g., Affolter et al., 2015; Uemura et al., 2016). Furthermore, recent studies demonstrated that past ^{17}O-excess variations can be measured through the δ^{17}O values of calcite (Barkan et al., 2015; Passey et al., 2014). Thus, ^{17}O-excess changes are a promising proxy for reconstructing past relative humidity changes in tropical and subtropical regions.

With regard to mid- and low-latitude regions, an investigation in a dry African region showed that the ^{17}O-excess in precipitation is strongly influenced by re-evaporation during convective activity (Landais et al., 2010). In the United States, the spatial distribution of ^{17}O-excess based on tap waters (Li et al., 2015) and a 2-year monitoring campaign based on rainfall/snowfall collected from a single location (Tian et al., 2018) were reported, but a humidity reconstruction was not provided. We should note that the ^{17}O-excess signal in a humid climate is expected to preserve diffusional fractionation during evaporation with minimal additional isotopic fractionation caused by the re-evaporation of precipitation. However, to the best of our knowledge, no observational study has proven that the ^{17}O-excess in precipitation preserves normalized relative humidity information in oceanic moisture source regions.

In this study, to evaluate the ^{17}O-excess in precipitation as a proxy for investigating the relative humidity in oceanic moisture source regions, we measured the ^{17}O-excess in precipitation falling over the subtropical island of Okinawa, Japan. The precipitation on this island is an ideal sample for such an evaluation because (i) the high humidity in the air minimizes raindrop re-evaporation effect, and (ii) the strong East Asian monsoon results in large seasonal variations in the relative humidity throughout the oceanic moisture source regions. In this paper, we present a two-year record of the ^{17}O-excess in the precipitation on a subtropical maritime island. To test the accuracy of the ^{17}O-excess measurements, the isotope ratios are calibrated carefully with respect to international references. The ^{17}O-excess data are compared with those from an arid region to investigate the magnitude of the rain re-evaporation effect. We reconstruct the normalized relative humidity in oceanic moisture source regions from the ^{17}O-excess data using a simple evaporation model based on a closure assumption. Then, the reconstructed humidity based on ^{17}O-excess is compared with the observational humidity data in the moisture source oceans based on backward trajectory analyses. Finally, the influences of possible processes other than the evaporation and the uncertainty caused by the definition of ^{17}O-excess are also discussed.

2. Methods

2.1. Rainwater samples and meteorological data

Precipitation samples were collected weekly from January 2011 to December 2012 on the roof of the Okinawa Prefectural Institute of Health and Environment at Oozato in the southern part of Okinawa Island (officially called Okinawa-jima; “jima” means island in Japanese), Japan (26°11′11″N, 127°45′13″E, 90 m above mean sea level; Fig. 1). The sampling procedure was described in detail in a previous study (Uemura et al., 2012), in which the same samples were used for δ^{18}O and δD analyses. The precipitation samples were collected using a sampling machine whose lid is opened automatically when it rains. This system minimizes secondary evaporation and contamination from dry deposition of atmospheric dust. We measured 95 samples for which a sufficient amount of precipitation (>2.0 mL) was collected. Meteorological data were obtained at the Naha meteorological station, which is located 7 km to the northwest of the sampling site and is operated by the Japan Metrological Agency.

2.2. Definitions of the isotope ratios and ^{17}O-excess

The isotopic composition is expressed in units of per mill (‰) using delta notation ($\delta = R_{\mathrm{sample}}/R_{\mathrm{ref}} - 1$), where R is the isotopic ratio, and R_{sample} and R_{ref} are the isotopic ratios of the sample and reference water, respectively. ^{17}O-excess is defined by the following equation (Barkan and Luz, 2005) using logarithmic delta notation ($\delta' = \ln(\delta + 1) = \ln(R_{\mathrm{sample}}/R_{\mathrm{ref}})$):

$$^{17}\mathrm{O\text{-}excess} = \delta'^{17}\mathrm{O} - 0.528 \times \delta'^{18}\mathrm{O} \quad (1)$$

where ^{17}O-excess is indicated in units of per meg ($= 1 \times 10^{-6}$).

2.3. Isotope measurements

The δ^{17}O, δ^{18}O and δD values were measured simultaneously using a cavity ring-down spectrometer (L2140-i, Picarro Inc.) with a vaporizer unit (V1120-i, Picarro Inc.). The details of this laser spectrometer system were described in Steig et al. (2014). To obtain precise δ^{17}O values that are suitable for an evaluation of ^{17}O-excess, many repeated measurements are needed. Consequently, we used a 350 µL vial (C400-LV1, Thermo, National Scientific Ltd.), and the gap between the inner wall and outer wall of the vial was sealed with an epoxy resin to avoid evaporation.

One batch consists of 20 samples and two working standards (WSs). The WS is used to calibrate the data on the Vienna Standard Mean Ocean Water (VSMOW)-Standard Light Antarctic Precipitation (SLAP) scale. For each injection, 1 µL of liquid sample was used. A sample measurement was performed with 10 injections. For a WS measurement, 60 injections (i.e., 6 vials) were performed. Approximately 48 hours are required for one batch measurement. Memory effect corrections were applied to the isotope measurements (Gupta et al., 2009). Each sample was measured 3–6 times (i.e., in a total of 30–60 injections over 3–6 batches for each sample).

The uncertainty was estimated using the standard error of the mean ($1\sigma/\sqrt{n}$; hereafter SE). Based on the repeated measurements of the samples (i.e., the number of measurements, n, is 3–6), the uncertainties of the analyzed data are 0.007‰ for δ^{17}O, 0.008‰ for δ^{18}O and 0.05‰ for δD, and those of ^{17}O-excess and d-excess are 5 per meg and 0.09‰, respectively.

2.4. Calibration of δ^{17}O values

The isotope compositions were normalized onto the VSMOW-SLAP scale using a linear normalization method (Schoenemann et al., 2013); thus, the SLAP δ^{17}O value was assigned as −29.6986‰

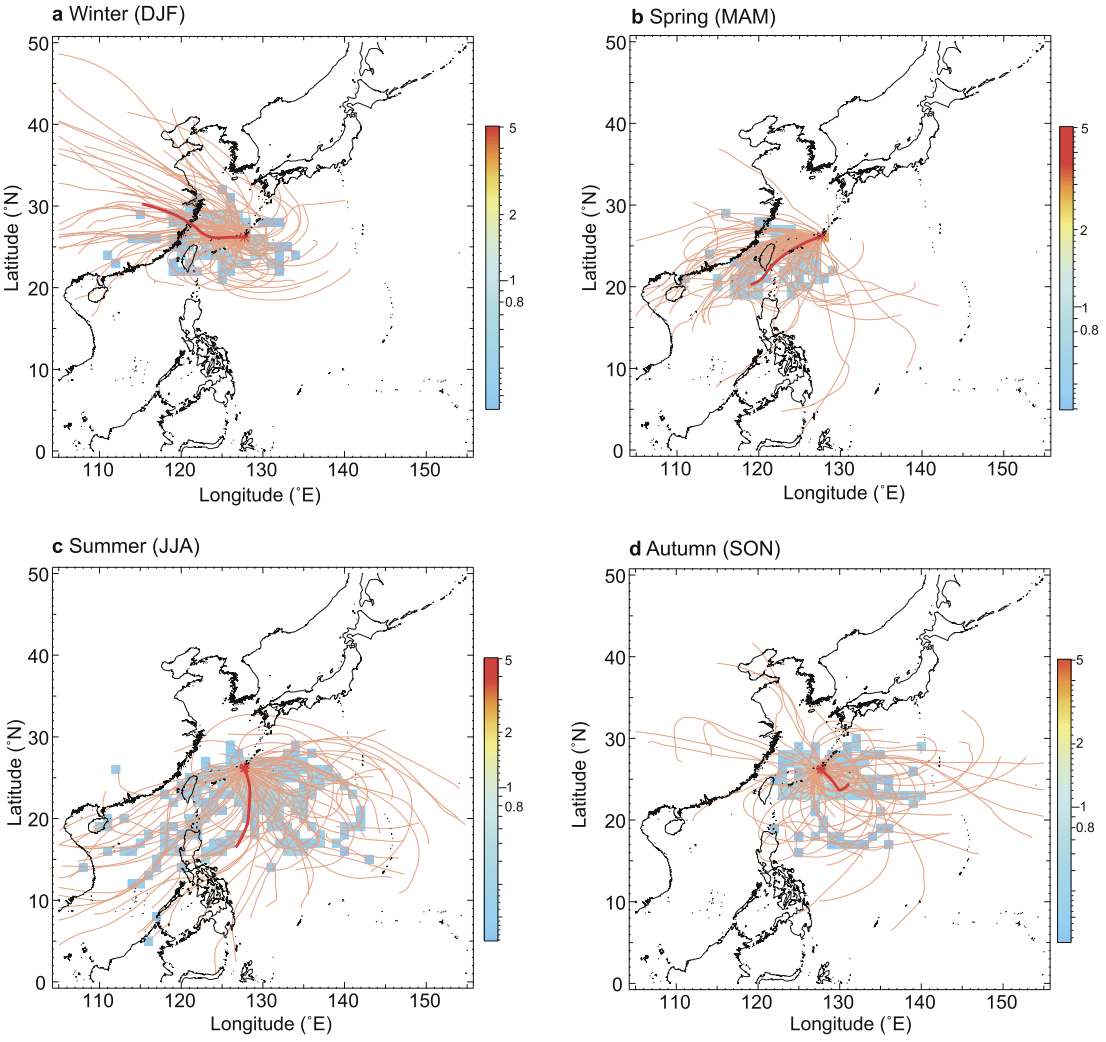

Fig. 1. Backward trajectory analysis for four seasons. (**a**) Backward trajectories (thin orange lines) and their average (bold red line) for the winter (DJF) season. (**b**) The same as (**a**) but for the spring (MAM). (**c**) The same as (**a**) but for the summer (JJA). (**d**) The same as (**a**) but for the autumn (SON). Colored grid points indicate the point density of the trajectory above the threshold value, and reflect the estimated moisture source area. The red star indicates the sampling location. (For interpretation of the colors in the figure(s), the reader is referred to the web version of this article.)

(vs. VSMOW). The isotope compositions of the laboratory WSs were carefully determined with international reference waters. Because the SLAP water was exhausted, we used SLAP2 water, whose $\delta^{18}O$ and $\delta^{17}O$ values are indistinguishable from those of the SLAP water (Lin et al., 2010). To minimize memory effects, five WSs with gradual differences in $\delta^{18}O$ values were measured between the VSMOW2 and SLAP2 waters. To evaluate the accuracy of our measurements, we also measured the Greenland Ice Sheet Precipitation (GISP) water provided by the International Atomic Energy Agency (IAEA) without assuming an assigned value. Each WS and IAEA reference water was measured by 50–150 injections; for the calibration, we adopted the averaged value of 20–60 injections from the latter measurement, where the memory effect was no longer observed. This sequence was performed 6 times; for example, 240 injections were performed to obtain the result for the GISP water.

2.5. Backward trajectory and ocean surface data

To compare the relative humidity in the moisture source region estimated from ^{17}O-excess, we calculated the observed relative humidity in the ocean. The moisture source region was evaluated by air mass backward trajectories, for which we used the Hybrid Single Particle Lagrangian Integrated Trajectory (HYSPLIT) model (Stein et al., 2015; https://ready.arl.noaa.gov/HYSPLIT.php). For all precipitation events (daily precipitation >0.5 mm) at the Naha meteorological station, the trajectory of the air mass (at 2000 m AGL) was calculated until 72 hours prior to the onset of precipitation.

The 72-hour was used as a standard case because an average time between moisture uptake in the boundary layer and the arrival of the air parcel over Greenland is 3–4 days based on a Lagrangian diagnostic model (Sodemann et al., 2008). However, a longer transport time (~7–9 days), is found in limited regions (Sodemann et al., 2008). Thus, the trajectories were also calculated for 10 days backward, which is about the maximum timescale on which integrity of the traced air parcel can be assumed (Pfahl and Wernli, 2008). In subtropical area, an average moisture residence time is ca. 10 days (Aggarwal et al., 2012). For sensitivity tests, different starting altitudes, 1000 m and 3000 m, were also calculated.

The moisture source area was determined based on point density of the trajectories (an hourly point on the trajectory was taken as a point). The threshold value was determined so that the cumulative percentage of the trajectories in $1^\circ \times 1^\circ$ grid points becomes 60%. Then, all the $1^\circ \times 1^\circ$ grid points above a threshold percentage are considered as the source area.

Then, the relative humidity in the moisture source region was calculated using an observational data set, namely, the International Comprehensive Ocean–Atmosphere Data Set (ICOADS; Freeman et al., 2017). The relative humidity normalized to the SST

in the oceanic moisture source region (h_n) was calculated using the 1° × 1° grid points data-set of SST and humidity from ICOADS. Land grid points were excluded from the calculation.

3. Results and discussion

3.1. ^{17}O-excess of the GISP water

The $\delta^{18}O$ and δD values of the GISP water are $-24.774 \pm 0.033‰$ ($\pm 1\sigma$) and $-189.39 \pm 0.30‰$, respectively. Accounting for the number of measurements, the uncertainties based on the SE are $\pm 0.007‰$ for $\delta^{18}O$ and $\pm 0.07‰$ for δD. For comparison, the IAEA recommended value for $\delta^{18}O$ is $-24.76 \pm 0.01‰$ ($\pm$SE), and that for δD is $-189.5 \pm 0.2‰$ ($\pm$SE) (IAEA, 2007). Thus, our $\delta^{18}O$ and δD values agree well with the international recommended values within their mutual error range, thereby certifying our calibration method.

The ^{17}O-excess value of the GISP water in this study is 33 ± 12 per meg ($\pm 1\sigma$). These ^{17}O-excess data exhibit a normal frequency distribution, suggesting negligible systematic error. Considering the number of repeated analyses, our ^{17}O-excess value for the GISP is 33 ± 2 per meg ($\pm$SE). For comparison, recent analyses using different methods reported values of 23 ± 2 per meg by off-axis integrated cavity output spectroscopy (Berman et al., 2013), 28 ± 4 per meg by isotope ratio mass spectroscopy (Schoenemann et al., 2013) and 27 ± 4 per meg by cavity ring-down spectroscopy (CRDS; Steig et al., 2014). The overall average of previous measurements after VSMOW-SLAP normalization is 27 ± 11 per meg ($\pm 1\sigma$) (Schoenemann et al., 2013). Thus, our data are consistent with the findings of previous studies within their mutual error ranges.

3.2. Backward trajectory analysis

The results of 72-hour backward trajectory analysis are shown in Fig. 1. The wind direction on Okinawa Island changes seasonally because of the East Asian monsoon. In the winter (December–February), the air masses mainly originate from the direction of the East China Sea (Fig. 1a). In contrast, during the summertime (June–August), most of the air masses come from the direction of the Pacific Ocean (Fig. 1c). Most of the air masses in the spring (March–May) originate from the southwest (Fig. 1b). The autumn season (September–November) marks a transition from summer to winter and thus shows scattered wind directions (Fig. 1d). Results of sensitivity tests for different starting altitudes ranged from 1000 m to 3000 m does not show significant changes for moisture source regions (Supplementary material, Fig. S1).

The oceanic moisture source region for precipitation, defined to reflect 60% of the point density of the trajectories, are shown in Fig. 1 (colored grid points). For example, the oceanic moisture source regions are the East China Sea for the winter, the area between the East China Sea and Philippine Sea for the spring, and the Philippine Sea for the summer and autumn.

The results of 10-day backward trajectory are shown in Supplementary material (Fig. S2). The seasonality of the wind direction is essentially the same as 72-hour results, but estimated moisture source regions are extended. For example, in summer, a part of moisture source region is extended to cover the Indian Ocean.

3.3. ^{17}O-excess in precipitation

The isotopic compositions of the precipitation on Okinawa Island and the meteorological data are shown in Fig. 2 and Supplementary Tables (Tables S1 and S2). Monthly isotope ratios were calculated by a precipitation-weighted average. Clear seasonal cycles were observed in the temperature and relative humidity, both

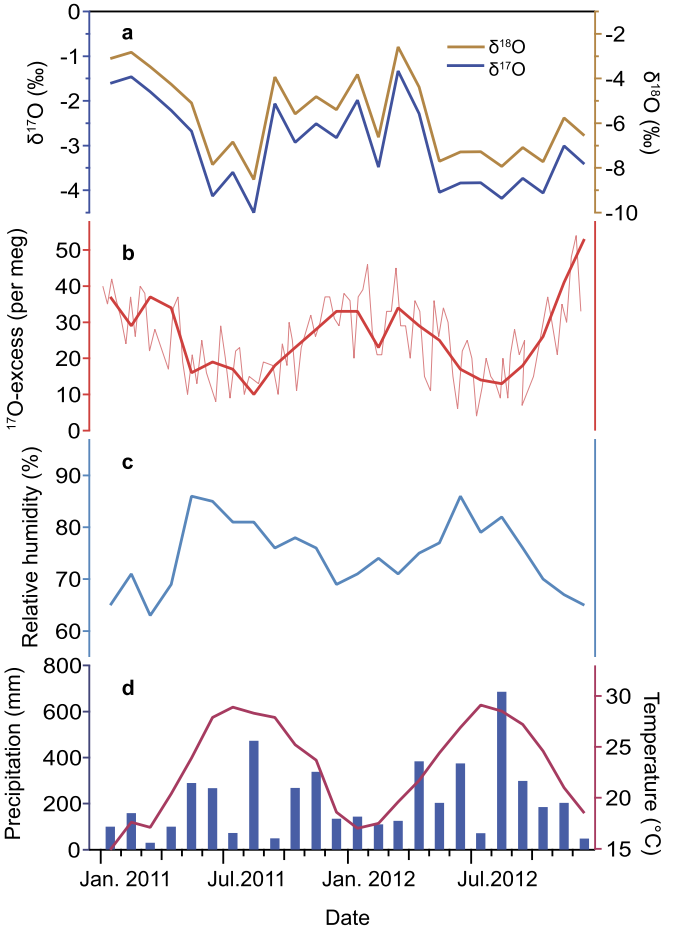

Fig. 2. Oxygen isotopic ratios in precipitation and meteorological data in Okinawa. (**a**) Monthly precipitation-weighted average values of $\delta^{18}O$ and $\delta^{17}O$ in precipitation. (**b**) Weekly ^{17}O-excess in precipitation (thin red line). The bold line indicates the monthly precipitation-weighted average of ^{17}O-excess. (**c**) Monthly relative humidity at the meteorological station. (**d**) Monthly precipitation amount (blue bar) and air temperature (red line) at the meteorological station.

of which were high during the summer and low during the winter. The amount of precipitation shows an irregular pattern but generally large values during the Meiyu/Baiu rainy season and summertime (April–September). Because the δD, $\delta^{18}O$ and d-excess results were previously discussed in Uemura et al. (2012), in this study, we focus on ^{17}O-excess variations. Accordingly, a clear seasonality in ^{17}O-excess was observed with low values in the summer (5–25 per meg) and high values in the winter (25–50 per meg).

3.4. Humidity at the sampling site versus ^{17}O-excess

The ^{17}O-excess in the precipitation on Okinawa Island exhibits a negative correlation with the relative humidity (Fig. 3), which is consistent with the prediction of an evaporation model in the ocean (Barkan and Luz, 2007). Because Okinawa Island is surrounded by the ocean, the humidity at the Naha meteorological station (3 km from the coast) is expected to be influenced largely by the changes in relative humidity in the moisture source ocean. Furthermore, the negative correlation between the Okinawa ^{17}O-excess and relative humidity is similar to the correlation found in measurements of marine water vapor from the Southern Indian Ocean and the Southern Ocean (Uemura et al., 2010).

In contrast, a raindrop re-evaporation effect was observed in the precipitation ^{17}O-excess over West Africa (Landais et al., 2010). Lower observed ^{17}O-excess values under conditions of lower humidity mainly result from the re-evaporation of raindrops; as

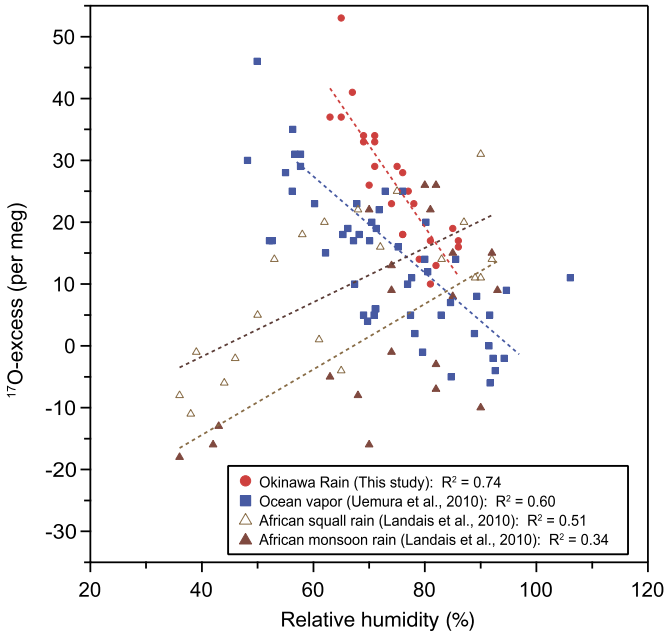

Fig. 3. ^{17}O-excess versus the relative humidity at sampling sites. ^{17}O-excess in the precipitation on Okinawa Island against relative humidity data at the Naha meteorological station (red circle). The blue square indicates the ^{17}O-excess in atmospheric water vapor in the Southern Ocean against the relative humidity at the sampling sites (Uemura et al., 2010). Triangles indicate the ^{17}O-excess in the precipitation in West Africa against the relative humidity at the sampling sites for three-month observations (deep brown) and for a squall event (light brown) (Landais et al., 2010). Dotted lines indicate linear regressions of each data set. Note that the data are plotted against the relative humidity instead of h_n.

a result, the precipitation ^{17}O-excess correlates positively with the relative humidity at the sampling site (Fig. 3). In a raindrop re-evaporation model (Bony et al., 2008), the intensity of re-evaporation is very low under a high relative humidity, and the droplets and the surrounding water vapor are close to isotopic equilibrium. The effect of the re-evaporation of raindrops at the sampling site would be negligible because of the high humidity on Okinawa Island. Therefore, the observed negative correlation between the Okinawa ^{17}O-excess and relative humidity suggests insignificant influence of a raindrop evaporation process on Okinawa Island.

3.5. Observational humidity in the source oceans

To compare the relative humidity reconstructed from ^{17}O-excess, we calculate the relative humidity normalized to the SST (h_n) in the moisture source oceans. We should note that h_n reconstructed from ^{17}O-excess does not represent the common relative humidity; rather, it denotes the relative humidity normalized to the saturation pressure at the SST in the oceanic moisture source region. A combined ICOADS h_n record in the moisture source region was constructed by connecting the h_n values for each season (Fig. 4a). On average, variability of the monthly mean values within a moisture source region based on the 3-day backward analysis (i.e., spatial variability of the temporal mean within the region) is 9% (1σ).

The h_n values for the moisture source areas are similar to relative humidity data at Naha meteorological station, except for those during the winter; the difference between the h_n values in moisture source areas and relative humidity at the station reaches 10%. During the wintertime, a very dry monsoon wind originates from the continent, and a warm Kuroshio Current supplies moisture to the dry air. In fact, a very large latent heat flux was observed in the East China Sea during the winter (Uemura et al., 2012).

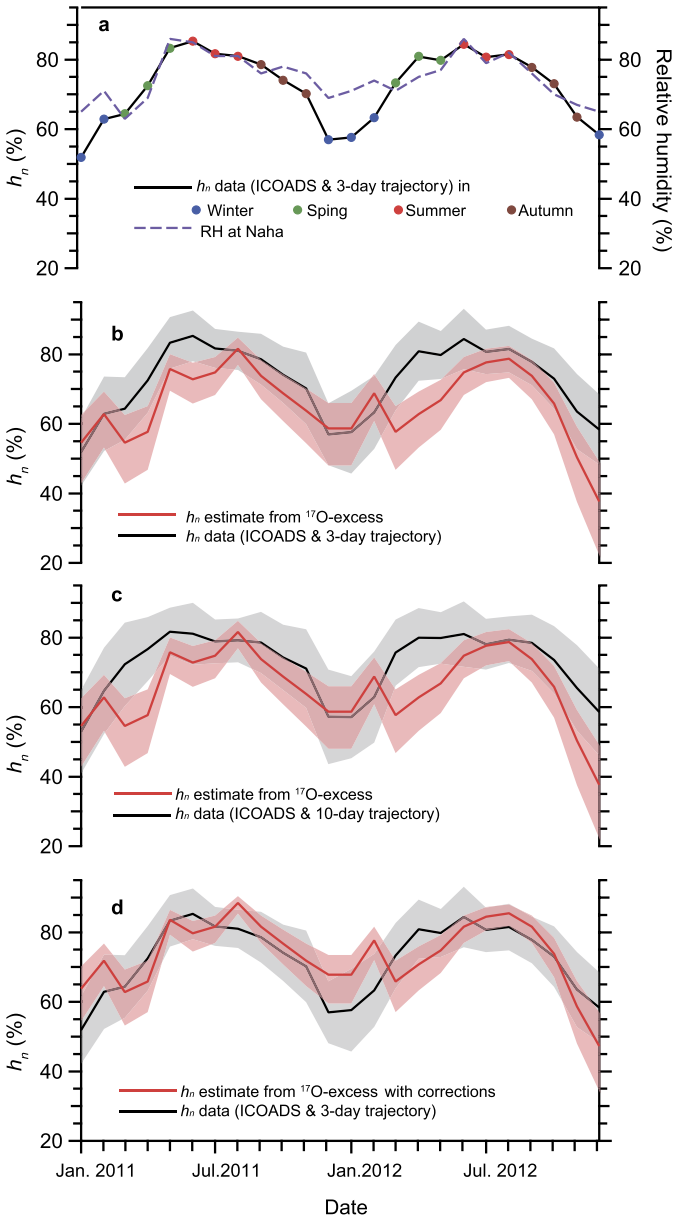

Fig. 4. Reconstructed normalized humidity in the oceanic moisture source regions. (**a**) Observed h_n in the oceanic moisture source regions for the winter (blue), spring (green), summer (red), and autumn (brown). Relative humidity at Naha (dotted purple). (**b**) The h_n estimate from ^{17}O-excess in precipitation (red line) with uncertainty (red shaded area). The uncertainty was estimated based on uncertainty of $^{18}\alpha_{\text{diff}}$ (i.e., 1.0096 ± 0.0018) and analytical error of ^{17}O-excess. The h_n from ICOADS data set in the moisture source regions based on the 3-day backward trajectory analysis (black line) with uncertainties (black shaded area). (**c**) The same as (**b**) but for the h_n from ICOADS data set in the moisture source regions were calculated based on the 10-day backward trajectory analysis (black line). (**d**) The same as (**b**) but the h_n estimate from ^{17}O-excess in precipitation (red line) is corrected for other effects (precipitation, closure assumption and ocean water isotopic composition).

These unique conditions (i.e., dry air over a relatively warm ocean) results in very low h_n values in the source region during the winter.

The h_n values in moisture source regions based on 10-day backward analysis (Fig. 4c) is very similar to those based on 3-day backward analysis (Fig. 4b). In addition, the values of h_n of moisture source regions based on the different starting altitudes (Fig. S1) agree within ±1%. These results suggest that the h_n estimate is not sensitive to the calculational conditions for backward trajectory analysis.

3.6. Source humidity estimate based on evaporation model

We evaluate a consistency between the humidity reconstructed from ^{17}O-excess in precipitation and humidity in oceanic moisture source regions. Based on a closure assumption (i.e., that vapor in the boundary layer originates from evaporation only) (Merlivat and Jouzel, 1979), the h_n can be related to ^{17}O-excess in oceanic water vapor (^{17}O-excess$_{(v)}$) as follows (Barkan and Luz, 2007):

$$^{17}\text{O-excess}_{(v)} = -\ln\left\{{}^{18}\alpha_{eq}^{0.529}\left({}^{18}\alpha_{diff}^{0.518}(1-h_n)+h_n\right)\right\} + 0.528\ln\left\{{}^{18}\alpha_{eq}\left({}^{18}\alpha_{diff}(1-h_n)+h_n\right)\right\} \quad (2)$$

where $^{18}\alpha_{eq}$ and $^{18}\alpha_{diff}$ respectively indicate equilibrium and diffusional fraction factors for ^{18}O/^{16}O. The $^{18}\alpha_{diff}$ was determined to be 1.0096 ± 0.0018 based on observations of water vapor in the ocean (Luz and Barkan, 2010; Uemura et al., 2010).

The sensitivity of reconstructed h_n to α_{diff} depends on absolute value of h_n; the uncertainty of h_n reconstruction decreases in higher humidity condition because of weaker contribution of diffusional fractionation. For example, the uncertainty of h_n estimate caused by that of α_{diff} (i.e., ±0.0018) ranges from ±4% (at 81% of h_n) to ±14% (at 38% of h_n) (±8% on average). Although $^{18}\alpha_{eq}$ depends on the temperature, this temperature dependence has little influence on the reconstructed h_n. For example, the estimates of h_n varied only by 1% when the values of $^{18}\alpha_{eq}$ changed from 1.00979 to 1.00897 (corresponding to SST changed from 20 to 30 °C). Thus, we calculated h_n with a constant $^{18}\alpha_{eq}$ (at SST of 25 °C) and with the measured ^{17}O-excess in the precipitation using Eq. (2).

The h_n estimates derived from the ^{17}O-excess data based on Eq. (2) are shown in Fig. 4b. The h_n reconstructed from ^{17}O-excess data shows a high correlation with the combined h_n record in the moisture source areas based on the 3-day backward trajectory analysis (slope = 0.74, $R^2 = 0.60$, $p < 0.01$). Although there is an offset of h_n (7% on average) between them, the seasonal amplitude (and its phase) of h_n are consistent with each other within their mutual uncertainty range.

A similarly high correlation is also found between the h_n data based on the 10-day backward trajectory analysis and the h_n derived from ^{17}O-excess ($R^2 = 0.48$; Fig. 4c). These results suggest that the h_n reconstructed from the ^{17}O-excess in precipitation is consistent with the h_n in the oceanic moisture source area. We should note, however, Eq. (2) estimates ^{17}O-excess of water vapor in the moisture source region. Other processes that may affect ^{17}O-excess in precipitation will be discussed in next section.

3.7. Source humidity estimate corrected for other processes

Besides evaporation in the moisture source region, ^{17}O-excess of precipitation can vary with the temperature of precipitation formation. A further increase of ^{17}O-excess is caused by the fact that the equilibrium fractionation slope of 0.529 is slightly higher than that of meteoric water line (0.528) (Luz and Barkan, 2010). This effect is larger at lower precipitation forming temperature. Luz and Barkan (2010) estimated that the ^{17}O-excess increases by 17 and 23 per meg for precipitation forming at −10 and −40 °C, respectively.

Here, we simply estimate an isotope ratio of initial small amount of precipitation (R_{p0}) formed under isotopic equilibrium with surrounding vapor (i.e., $R_{p0} = R_{v0} \cdot {}^{18}\alpha_{eq}$). The isotope ratio of initial vapor (R_{v0}) was obtained using the evaporation model (Eq. (2)). For example, under summer-time evaporation conditions (SST = 28 °C and RH = 80%), the ^{17}O-excess of an initial precipitation at dewpoint temperature (24 °C) is larger than that of corresponding vapor by 9 per meg. For winter-time evaporation conditions (SST = 21 °C and RH = 60%), the ^{17}O-excess in the 1st precipitation at dewpoint temperature (12 °C) is larger than that of corresponding vapor by 11 per meg. Thus, this minor seasonal amplitude of the precipitation effect (i.e., difference between winter and summer is 2 per meg) would not affect the seasonal amplitude of ^{17}O-excess of precipitation at the sampling site (difference between winter and summer is 20 per meg on average). However, these results suggest that temperature effect may cause systematic offset (ca. 9–11 per meg) between the vapor and precipitation.

Another potential bias of ^{17}O-excess evaporation model may be caused by the closure assumption used in the derivation of Eq. (2) (Merlivat and Jouzel, 1979). Only a few studies have investigated this problem on ^{17}O-excess, but an observation of d-excess in water vapor in the subtropical North Atlantic suggests that mixing in the boundary layer may affect the negative correlation between d-excess and h_n (Benetti et al., 2015). A recent study on d-excess suggested that the closure assumption is valid during strong large-scale ocean evaporation (such an event is characterized by low h_n of ca. 50%) but is most likely not fulfilled under high h_n conditions (Aemisegger and Sjolte, 2018). A single-column isotopic model suggests that the closure assumption results in lower ^{17}O-excess in the boundary layer by 3 per meg due to vapor flux from unsaturated downdraft into the boundary layer (Risi et al., 2010). Although this level of difference is within the analytical uncertainty, this effect also may add a systematic offset between the observed h_n and the h_n reconstructed based on the closure assumption model.

Finally, ^{17}O-excess of the ocean water also should be considered. Eq. (2) is derived on the assumption that ^{17}O-excess of the ocean water is the same as that of VSMOW. A measurement of ocean surface water from the Pacific and Atlantic oceans showed that the ^{17}O-excess of ocean water with respect to VSMOW (^{17}O-excess$_{(ocean/VSMOW)}$) is −5 per meg (Luz and Barkan, 2010). Since there is no spatial and temporal data set of ^{17}O-excess of the ocean water in the moisture source regions of this study, we used the averaged value of −5 per meg for correction.

Considering these factors, we re-evaluate the h_n reconstruction based on the ^{17}O-excess in precipitation. The ^{17}O-excess of vapor correcting for closure assumption bias ($\Delta_{closure}$ = 3 per meg) and ^{17}O-excess$_{(ocean/VSMOW)}$ can be written as follows:

$$^{17}\text{O-excess}_{(v\_cor)} = {}^{17}\text{O-excess}_{(v)} + \Delta_{closure} + {}^{17}\text{O-excess}_{(ocean/VSMOW)} \quad (3)$$

where ^{17}O-excess$_{(v_cor)}$ indicates the corrected ^{17}O-excess of vapor. Then, ^{17}O-excess of the initial precipitation (^{17}O-excess$_{(p)}$) is expressed by the following:

$$^{17}\text{O-excess}_{(p)} = {}^{17}\text{O-excess}_{(v\_cor)} + \Delta_{prep}. \quad (4)$$

Here, the value of precipitation effect (Δ_{prep}) ranges from 9 per meg (for summer) and 10 per meg (for spring and autumn) to 11 per meg (for winter).

The h_n reconstruction based on Eqs. (3) and (4) are shown in Fig. 4d. Seasonality and its amplitude are essentially the same as the h_n reconstruction based on Eq. (2). However, the absolute value of h_n shows an excellent agreement with the h_n from ICOADS observation. The average h_n offset between the ^{17}O-excess based estimate and the observation is only −1 %, which is smaller than the offset based on Eq. (2) (i.e., 7%). This result suggests that the potential influences on the ^{17}O-excess of precipitation other than the simple evaporation effect would not significantly affect the accuracy of the h_n reconstruction because the sum of the correction factors is not large (7 to 9 per meg). Rather, the correction improves the accuracy of h_n reconstruction.

Although we attempted to estimate the potential size of influences on the ^{17}O-excess other than evaporation, there are

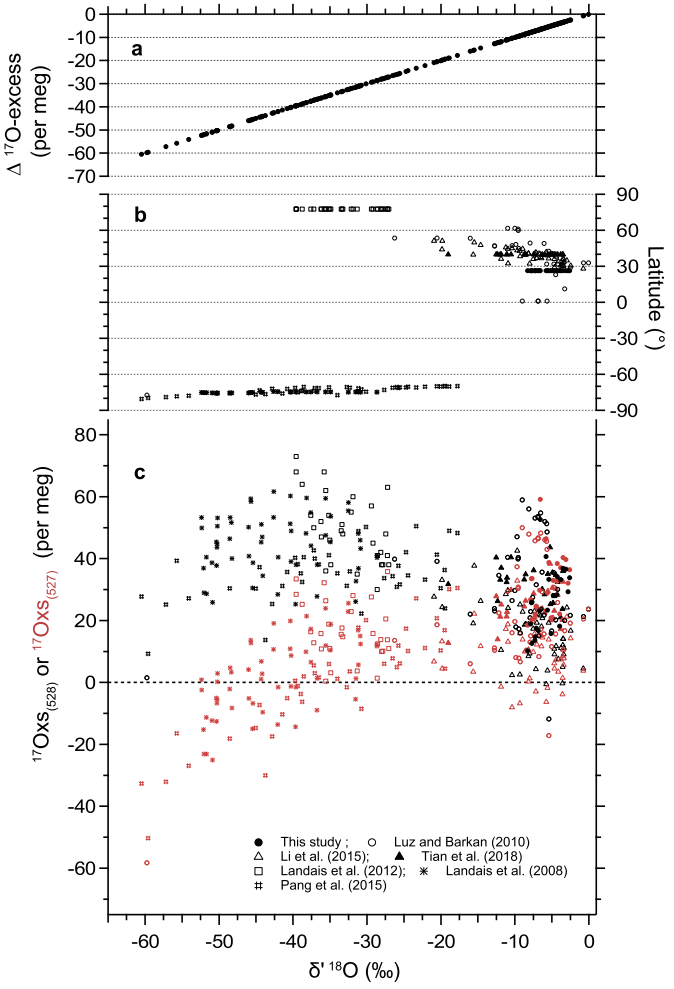

Fig. 5. Different definitions of ^{17}O-excess against δ'^{18}O. (**a**) Δ^{17}Oxs, defined as the difference between ^{17}Oxs$_{(527)}$ and ^{17}Oxs$_{(528)}$. (**b**) Latitudes of te sampling locations. Positive values indicate the Northern Hemisphere, and negative values indicate the Southern Hemisphere. (**c**) ^{17}Oxs$_{(528)}$ (black symbols) and ^{17}Oxs$_{(527)}$ (red symbols) in rainwater and snow samples; also shown are Okinawa rainwater (black circle; this study), Antarctic surface snow (asterisk; Landais et al., 2008), Antarctic surface snow (hash mark; Pang et al., 2015, a shallow ice core drilled at the North Greenland Eemian Ice Drilling (NEEM) site in Greenland (open square; Landais et al., 2012b), rain and snow of diverse provenance (open circle; Luz and Barkan, 2010), tap water in the United States (open triangle; Li et al., 2015), and rain and snow in the central United States (black triangle; Tian et al., 2018). For the tap water data, tap water data whose d-excess values are consistent with (within 5.2‰) interpolated local precipitation values were used.

still other factors such as; cloud type, condensation temperature, ^{17}O-excess in background atmosphere, and ^{17}O-excess in regional ocean surface water. To better constrain these factors and processes, further regional observations based on individual rain events will be useful.

3.8. Robustness against different definitions

For the ^{17}O-excess definition of meteoric water, the δ'^{17}O–δ'^{18}O slope of 0.528 has been widely adopted (Luz and Barkan, 2010; Meijer and Li, 1998). Recently, Miller (2018) noted that the δ'^{17}O–δ'^{18}O slope of the global meteoric water line is reduced from the common value of 0.528 to 0.5268–0.5270 after removing Antarctic data points (where the δ^{18}O value is smaller than −50‰). Therefore, in temperate and tropical regions, the δ'^{17}O–δ'^{18}O slope should be significantly smaller than 0.528.

To evaluate the impact of this hypothesized lower slope, we calculate values of ^{17}O-excess with different slopes. For clarity, the ^{17}O-excess with a smaller slope of 0.527 is denoted as ^{17}Oxs$_{(527)}$ ($= \delta'^{17}\mathrm{O} - 0.527 \times \delta'^{18}\mathrm{O}$). In contrast, the commonly used ^{17}O-excess calculated by a slope of 0.528 is denoted as ^{17}Oxs$_{(528)}$ only in this section and Fig. 5. The impacts of the different slopes on ^{17}O-excess are illustrated in Fig. 5. The difference between them, namely, Δ^{17}Oxs ($= {}^{17}\mathrm{Oxs}_{(527)} - {}^{17}\mathrm{Oxs}_{(528)}$), gradually expands by ca. 1 per meg per 1‰ of δ^{18}O as δ^{18}O decreases (Fig. 5a and 5c).

The δ^{18}O values decrease significantly in polar regions (absolute latitude > 60°; Fig. 5b). The absolute value of ^{17}O-excess in polar regions is very sensitive to small changes in the slope, i.e., Δ^{17}Oxs is −50 per meg at a δ^{18}O value of −50‰. This sensitivity to the slope causes fundamental difficulties in interpreting the absolute value of ^{17}Oxs$_{(528)}$ in polar regions. In contrast, in the region where δ^{18}O is greater than −10‰, Δ^{17}Oxs is smaller than 10 per meg, which is close to the typical analytical uncertainty of ^{17}O-excess measurements. We should note that δ^{18}O is greater than −10‰ in most tropical and subtropical regions (i.e., between 35°S and 35°N) (e.g., Bowen and Wilkinson, 2002). For example, the average Δ^{17}Oxs of our observations in Okinawa is −6 per meg. Therefore, this analysis shows that ^{17}Oxs$_{(528)}$ values in tropical and subtropical regions are insensitive to changes in the slope and thus constitute a reliable tracer for the hydrological cycle.

In addition to the impacts of different slopes, the overall trend of ^{17}Oxs$_{(528)}$ shown in Fig. 5c invokes a fundamental question regarding the global distribution of ^{17}Oxs$_{(528)}$. Specifically, ^{17}Oxs$_{(528)}$ shows a clear increasing trend from 20 per meg to 50 per meg when the δ^{18}O values decrease from −10‰ to −40‰. Interestingly, this trend is similar to water vapor observations at Alert, Canada (Lin et al., 2013). Lin et al. (2013) interpreted that this anomaly originated from stratospheric water vapor, although this conclusion was criticized on the basis of its precision (Miller, 2013); mathematically, ^{17}Oxs$_{(528)}$ increased gradually as the δ^{18}O values decreased simply because it was calculated against a slope of 0.528 despite the fact that the δ'^{17}O–δ'^{18}O slope of the global meteoric water line (excluding Antarctic data points) is lower than 0.528. Similarly, the strong anticorrelation between ^{17}Oxs$_{(528)}$ and δ^{18}O found in Greenland (δ^{18}O ranges from −38‰ to −28‰; Landais et al., 2012b) and in the United States (δ^{18}O ranges from −5 to −25‰; Li et al., 2015) will be reduced if one adopts a slope of 0.527 instead of 0.528. These results suggest that the increasing trend in ^{17}Oxs$_{(528)}$ alone is not strong evidence for stratospheric input because of its sensitivity to small changes in the ^{17}O-excess definition.

In polar regions, the ^{17}Oxs$_{(528)}$ of snow decreases along with a lower δ^{18}O value. ^{17}Oxs$_{(528)}$ decreases in polar high plateau regions, where the δ^{18}O value is lower than −50‰. In fact, a very small ^{17}Oxs$_{(528)}$ (< −20 per meg) was observed at Vostok (where δ^{18}O < −50‰) in Antarctica (Landais et al., 2012a). The mechanisms underlying this phenomenon are still unclear, but the influences of diffusional fractionation during snow formation (Landais et al., 2012a) and the precipitation regime (Miller, 2018) have been suggested. The presence of this local decreasing trend complicates the interpretation of Antarctic ice core data, particularly at remote inland sites (Winkler et al., 2012). This phenomenon remains even after incorporating ^{17}Oxs$_{(527)}$, suggesting that this local effect cannot be explained by the lower δ'^{17}O–δ'^{18}O slope. In addition, Δ^{17}Oxs reaches ca. −50 per meg at a δ^{18}O value of −50‰. This indicates that absolute values of ^{17}O-excess in polar regions are highly sensitive to its definition.

In summary, in regions with low δ^{18}O values such as Antarctica, small changes in the slope affect the absolute value of ^{17}Oxs$_{(528)}$, and thus, additional difficulties are expected during the interpretation of ^{17}Oxs$_{(528)}$ data. In contrast, the impact of uncertainty in the slope is minimized in tropical and subtropical regions where the δ^{18}O value is usually large (> −10‰).

4. Conclusions

The ^{17}O-excess in precipitation on Okinawa Island showed a clear seasonal variation. The relative humidity normalized to the SST (denoted as h_n) in the oceanic moisture source region was reconstructed from the ^{17}O-excess in the precipitation using the simple evaporation model. Interestingly, the reconstructed h_n is consistent with the h_n observed in the oceanic moisture source region. After correcting for the bias caused by closure assumption, the precipitation effect and ^{17}O-excess values of ocean-water, the reconstructed h_n shows a better agreement with the h_n in the oceanic moisture source region. Furthermore, a sensitivity test revealed that the ^{17}O-excess values in most tropical and subtropical regions will not be significantly affected by different slope definitions for ^{17}O-excess because of its higher δ'^{18}O value. These results suggest that the ^{17}O-excess in the precipitation on Okinawa Island is dominantly controlled by h_n in the moisture source region through variances in the strength of diffusional isotope fractionation. Therefore, the ^{17}O-excess in humid tropical and subtropical regions is an important and unique tracer for investigating past and present hydrogeological cycles because it provides a quantitative estimate of the relative humidity in the oceanic moisture source region. The findings presented here also suggest that analyses of fluid inclusions (e.g., water) in speleothems and/or ^{17}O in calcite will be useful as a quantitative proxy for paleoclimate variations.

Acknowledgements

We thank the Okinawa Prefectural Institute of Health and Environment for sharing the rainwater samples. We also thank Makoto Watanabe of Sanyo Furue Science Corporation for technical advice for Picarro analyzer. This research was supported by JSPS and MEXT KAKENHI Grant Numbers: JP15H01729 and JP17KK0012.

Appendix A. Supplementary material

Supplementary material related to this article can be found online at https://doi.org/10.1016/j.epsl.2019.02.012.

References

Aemisegger, F., Sjolte, J., 2018. A climatology of strong large-scale ocean evaporation events. Part II: relevance for the deuterium excess signature of the evaporation flux. J. Climate 31, 7313–7336.

Affolter, S., Häuselmann, A.D., Fleitmann, D., Häuselmann, P., Leuenberger, M., 2015. Triple isotope (δD, δ^{17}O, δ^{18}O) study on precipitation, drip water and speleothem fluid inclusions for a Western Central European cave (NW Switzerland). Quat. Sci. Rev. 127, 73–89.

Aggarwal, P.K., Alduchov, O.A., Froehlich, K.O., Araguas-Araguas, L.J., Sturchio, N.C., Kurita, N., 2012. Stable isotopes in global precipitation: a unified interpretation based on atmospheric moisture residence time. Geophys. Res. Lett. 39.

Angert, A., Cappa, C.D., DePaolo, D.J., 2004. Kinetic ^{17}O effects in the hydrologic cycle: indirect evidence and implications. Geochim. Cosmochim. Acta 68, 3487–3495.

Barkan, E., Luz, B., 2005. High precision measurements of ^{17}O/^{16}O and ^{18}O/^{16}O ratios in H_2O. Rapid Commun. Mass Spectrom. 19, 3737–3742.

Barkan, E., Luz, B., 2007. Diffusivity fractionations of $H_2{}^{16}O/H_2{}^{17}O$ and $H_2{}^{16}O/H_2{}^{18}O$ in air and their implications for isotope hydrology. Rapid Commun. Mass Spectrom. 21, 2999–3005.

Barkan, E., Musan, I., Luz, B., 2015. High-precision measurements of δ^{17}O and ^{17}O-excess of NBS19 and NBS18. Rapid Commun. Mass Spectrom. 29, 2219–2224.

Benetti, M., Aloisi, G., Reverdin, G., Risi, C., Sèze, G., 2015. Importance of boundary layer mixing for the isotopic composition of surface vapor over the subtropical North Atlantic Ocean. J. Geophys. Res., Atmos. 120, 2190–2209.

Berman, E.S., Levin, N.E., Landais, A., Li, S., Owano, T., 2013. Measurement of δ^{18}O, δ^{17}O, and ^{17}O-excess in water by off-axis integrated cavity output spectroscopy and isotope ratio mass spectrometry. Anal. Chem. 85, 10392–10398.

Bony, S., Risi, C., Vimeux, F., 2008. Influence of convective processes on the isotopic composition (δ^{18}O and δD) of precipitation and water vapor in the tropics: 1. Radiative-convective equilibrium and Tropical Ocean–Global Atmosphere–Coupled Ocean–Atmosphere Response Experiment (TOGA–COARE) simulations. J. Geophys. Res. 113.

Bowen, G.J., Wilkinson, B., 2002. Spatial distribution of δ^{18}O in meteoric precipitation. Geology 30.

Craig, H., 1961. Isotopic variations in meteoric waters. Science 133, 1702–1703.

Dansgaard, W., 1964. Stable isotopes in precipitation. Tellus 16, 436–468.

Freeman, E., Woodruff, S.D., Worley, S.J., Lubker, S.J., Kent, E.C., Angel, W.E., Berry, D.I., Brohan, P., Eastman, R., Gates, L., Gloeden, W., Ji, Z., Lawrimore, J., Rayner, N.A., Rosenhagen, G., Smith, S.R., 2017. ICOADS release 3.0: a major update to the historical marine climate record. Int. J. Climatol. 37, 2211–2232.

Gupta, P., Noone, D., Galewsky, J., Sweeney, C., Vaughn, B.H., 2009. Demonstration of high-precision continuous measurements of water vapor isotopologues in laboratory and remote field deployments using wavelength-scanned cavity ringdown spectroscopy (WS-CRDS) technology. Rapid Commun. Mass Spectrom. 23, 2534–2542.

IAEA, 2007. Reference sheet for reference material, GISP.

Jouzel, J., 2013. A brief history of ice core science over the last 50 yr. Clim. Past 9, 2525–2547.

Landais, A., Barkan, E., Luz, B., 2008. Record of δ^{18}O and ^{17}O-excess in ice from Vostok Antarctica during the last 150,000 years. Geophys. Res. Lett. 35, L02709.

Landais, A., Ekaykin, A., Barkan, E., Winkler, R., Luz, B., 2012a. Seasonal variations of ^{17}O-excess and d-excess in snow precipitation at Vostok station, East Antarctica. J. Glaciol. 58, 725–733.

Landais, A., Risi, C., Bony, S., Vimeux, F., Descroix, L., Falourd, S., Bouygues, A., 2010. Combined measurements of ^{17}O-excess and d-excess in African monsoon precipitation: implications for evaluating convective parameterizations. Earth Planet. Sci. Lett. 298, 104–112.

Landais, A., Steen-Larsen, H.C., Guillevic, M., Masson-Delmotte, V., Vinther, B., Winkler, R., 2012b. Triple isotopic composition of oxygen in surface snow and water vapor at NEEM (Greenland). Geochim. Cosmochim. Acta 77, 304–316.

Li, S., Levin, N.E., Chesson, L.A., 2015. Continental scale variation in ^{17}O-excess of meteoric waters in the United States. Geochim. Cosmochim. Acta 164, 110–126.

Lin, Y., Clayton, R.N., Gröning, M., 2010. Calibration of δ^{17}O and δ^{18}O of international measurement standards – VSMOW, VSMOW2, SLAP, and SLAP2. Rapid Commun. Mass Spectrom. 24, 773–776.

Lin, Y., Clayton, R.N., Huang, L., Nakamura, N., Lyons, J.R., 2013. Oxygen isotope anomaly observed in water vapor from Alert, Canada and the implication for the stratosphere. Proc. Natl. Acad. Sci. USA 110, 15608–15613.

Luz, B., Barkan, E., 2010. Variations of ^{17}O/^{16}O and ^{18}O/^{16}O in meteoric waters. Geochim. Cosmochim. Acta 74, 6276–6286.

Meijer, H.A.J., Li, W.J., 1998. The use of electrolysis for accurate δ^{17}O and δ^{18}O isotope measurements in water. Isot. Environ. Health Stud. 34, 349–369.

Merlivat, L., Jouzel, J., 1979. Global climatic interpretation of the deuterium–oxygen 18 relationship for precipitation. J. Geophys. Res. 84, 5029–5033.

Miller, M.F., 2013. Oxygen isotope anomaly not present in water vapor from Alert, Canada. Proc. Natl. Acad. Sci. USA 110, E4567.

Miller, M.F., 2018. Precipitation regime influence on oxygen triple-isotope distributions in Antarctic precipitation and ice cores. Earth Planet. Sci. Lett. 481, 316–327.

Pang, H., Hou, S., Landais, A., Masson-Delmotte, V., Prie, F., Steen-Larsen, H.C., Risi, C., Li, Y., Jouzel, J., Wang, Y., He, J., Minster, B., Falourd, S., 2015. Spatial distribution of ^{17}O-excess in surface snow along a traverse from Zhongshan station to Dome A, East Antarctica. Earth Planet. Sci. Lett. 414, 126–133.

Passey, B.H., Hu, H., Ji, H., Montanari, S., Li, S., Henkes, G.A., Levin, N.E., 2014. Triple oxygen isotopes in biogenic and sedimentary carbonates. Geochim. Cosmochim. Acta 141, 1–25.

Pfahl, S., Wernli, H., 2008. Air parcel trajectory analysis of stable isotopes in water vapor in the eastern Mediterranean. J. Geophys. Res., Atmos. 113.

Risi, C., Landais, A., Bony, S., Jouzel, J., Masson-Delmotte, V., Vimeux, F., 2010. Understanding the ^{17}O-excess glacial–interglacial variations in Vostok precipitation. J. Geophys. Res. 115.

Schoenemann, S.W., Schauer, A.J., Steig, E.J., 2013. Measurement of SLAP2 and GISP δ^{17}O and proposed VSMOW-SLAP normalization for δ^{17}O and ^{17}O-excess. Rapid Commun. Mass Spectrom. 27, 582–590.

Schoenemann, S.W., Steig, E.J., Ding, Q., Markle, B.R., Schauer, A.J., 2014. Triple water-isotopologue record from WAIS Divide, Antarctica: controls on glacial–interglacial changes in ^{17}O excess of precipitation. J. Geophys. Res., Atmos. 119, 8741–8763.

Sodemann, H., Schwierz, C., Wernli, H., 2008. Interannual variability of Greenland winter precipitation sources: lagrangian moisture diagnostic and North Atlantic Oscillation influence. J. Geophys. Res., Atmos. 113.

Steen-Larsen, H.C., Masson-Delmotte, V., Hirabayashi, M., Winkler, R., Satow, K., Prié, F., Bayou, N., Brun, E., Cuffey, K.M., Dahl-Jensen, D., Dumont, M., Guillevic, M., Kipfstuhl, S., Landais, A., Popp, T., Risi, C., Steffen, K., Stenni, B., Sveinbjörnsdottír, A.E., 2014a. What controls the isotopic composition of Greenland surface snow? Clim. Past 10, 377–392.

Steen-Larsen, H.C., Sveinbjörnsdottir, A.E., Peters, A.J., Masson-Delmotte, V., Guishard, M.P., Hsiao, G., Jouzel, J., Noone, D., Warren, J.K., White, J.W.C., 2014b. Climatic controls on water vapor deuterium excess in the marine boundary layer of the North Atlantic based on 500 days of in situ, continuous measurements. Atmos. Chem. Phys. 14, 7741–7756.

Steig, E.J., Gkinis, V., Schauer, A.J., Schoenemann, S.W., Samek, K., Hoffnagle, J., Dennis, K.J., Tan, S.M., 2014. Calibrated high-precision ^{17}O-excess measurements

using cavity ring-down spectroscopy with laser-current-tuned cavity resonance. Atmos. Meas. Tech. 7, 2421–2435.

Stein, A.F., Draxler, R.R., Rolph, G.D., Stunder, B.J.B., Cohen, M.D., Ngan, F., 2015. NOAA's HYSPLIT atmospheric transport and dispersion modeling system. Bull. Am. Meteorol. Soc. 96, 2059–2077.

Tian, C., Wang, L., Kaseke, K.F., Bird, B.W., 2018. Stable isotope compositions δ^2H, δ^{18}O and δ^{17}O of rainfall and snowfall in the central United States. Sci. Rep. 8, 6712.

Touzeau, A., Landais, A., Stenni, B., Uemura, R., Fukui, K., Fujita, S., Guilbaud, S., Ekaykin, A., Casado, M., Barkan, E., Luz, B., Magand, O., Teste, G., Le Meur, E., Baroni, M., Savarino, J., Bourgeois, I., Risi, C., 2016. Acquisition of isotopic composition for surface snow in East Antarctica and the links to climatic parameters. Cryosphere 10, 837–852.

Uemura, R., Barkan, E., Abe, O., Luz, B., 2010. Triple isotope composition of oxygen in atmospheric water vapor. Geophys. Res. Lett. 37.

Uemura, R., Matsui, Y., Yoshimura, K., Motoyama, H., Yoshida, N., 2008. Evidence of deuterium excess in water vapor as an indicator of ocean surface conditions. J. Geophys. Res. 113, D19114.

Uemura, R., Motoyama, H., Masson-Delmotte, V., Jouzel, J., Kawamura, K., Goto-Azuma, K., Fujita, S., Kuramoto, T., Hirabayashi, M., Miyake, T., Ohno, H., Fujita, K., Abe-Ouchi, A., Iizuka, Y., Horikawa, S., Igarashi, M., Suzuki, K., Suzuki, T., Fujii, Y., 2018. Asynchrony between Antarctic temperature and CO_2 associated with obliquity over the past 720,000 years. Nat. Commun. 9, 961.

Uemura, R., Nakamoto, M., Asami, R., Mishima, S., Gibo, M., Masaka, K., Jin-Ping, C., Wu, C.-C., Chang, Y.-W., Shen, C.-C., 2016. Precise oxygen and hydrogen isotope determination in nanoliter quantities of speleothem inclusion water by cavity ring-down spectroscopic techniques. Geochim. Cosmochim. Acta 172, 159–176.

Uemura, R., Yonezawa, N., Yoshimura, K., Asami, R., Kadena, H., Yamada, K., Yoshida, N., 2012. Factors controlling isotopic composition of precipitation on Okinawa Island, Japan: implications for paleoclimate reconstruction in the East Asian Monsoon region. J. Hydrol. 475, 314–322.

Winkler, R., Landais, A., Sodemann, H., Dümbgen, L., Prié, F., Masson-Delmotte, V., Stenni, B., Jouzel, J., 2012. Deglaciation records of ^{17}O-excess in East Antarctica: reliable reconstruction of oceanic normalized relative humidity from coastal sites. Clim. Past 8, 1–16.